Biomedical Signal Processing and Control 8 (2013) 500–508

Contents lists available at ScienceDirect

Biomedical Signal Processing and Control

journal homepage: www.elsevier.com/locate/bspc

Individualized closed-loop control of propofol anesthesia: A preliminary study

Kristian Soltesz[a,*,1], Jin-Oh Hahn[b], Tore Hägglund[a,1], Guy A. Dumont[c], J. Mark Ansermino[d]

[a] Department of Automatic Control, Lund University, Box 118, SE-221 00 Lund, Sweden
[b] Department of Mechanical Engineering, The University of Maryland, College Park, MD 20742, USA
[c] Department of Electrical and Computer Engineering, The University of British Columbia, 3023 – 2332 Main Mall, V6T 1Z4 Vancouver, BC, Canada
[d] Department of Anesthesiology, Pharmacology and Therapeutics, The University of British Columbia and BC Children's Hospital, 1L7-4480 Oak Street, V6H 3V4 Vancouver, BC, Canada

ARTICLE INFO

Article history:
Received 28 September 2012
Received in revised form 11 February 2013
Accepted 16 April 2013
Available online 30 May 2013

Keywords:
Anesthesia
Automatic control
Individualized treatment

ABSTRACT

This paper proposes an individualized approach to closed-loop control of depth of hypnosis during propofol anesthesia. The novelty of the paper lies in the individualization of the controller at the end of the induction phase of anesthesia, based on a patient model identified from the dose–response relationship during induction of anesthesia. The proposed approach is shown to be superior to administration of propofol based on population-based infusion schemes tailored to individual patients. This approach has the potential to outperform fully adaptive approaches in regards to controller robustness against measurement variability due to surgical stimulation. To streamline controller synthesis, two output filters were introduced (inverting the Hill dose–response model and the linear time-invariant sensor model), which yield a close-to-linear representation of the system dynamics when used with a compartmental patient model. These filters are especially useful during the induction phase of anesthesia in which a nonlinear dose–response relationship complicates the design of an appropriate controller. The proposed approach was evaluated in simulation on pharmacokinetic and pharmacodynamic models of 44 patients identified from real clinical data. A model of the NeuroSense, a hypnotic depth monitor based on wavelet analysis of EEG, was also included. This monitor is similar to the well-known BIS, but has linear time-invariant dynamics and does not introduce a delay. The proposed scheme was compared with a population-based controller, i.e. a controller only utilizing models based on demographic covariates for its tuning. On average, the proposed approach offered 25% improvement in disturbance attenuation, measured as the integrated absolute error following a step disturbance. The corresponding standard deviation from the reference was also decreased by 25%. Results are discussed and possible directions of future work are proposed.

1. Introduction

The purpose of administering anesthetic drugs during surgical procedures is to prevent unintended intra-operative awareness and to preserve stable suppression of noxious stimulation on the circulatory and hormonal systems, and on occasion to provide muscle relaxation [1]. Accordingly, anesthetic drugs are categorized into hypnotics, analgesics and neuromuscular blocking drugs. The fulfillment of the above-mentioned objectives is complicated by highly patient-specific and uncertain dose–response dynamics [2], unpredictable disturbances introduced by surgical stimulation [3] and synergetic effects between drugs (e.g. hypnotic–opioid synergy) [4]. Additional constraints are imposed by the fact that some anesthetic drugs have undesirable side effects (e.g. cardiovascular depression, cognitive impairment, nausea, vomiting and respiratory depression). Thus, the drugs must be restrictively administered during surgical procedures [5].

The hypnosis profile is divided into three temporal phases. During the induction phase of anesthesia, the patient is transferred from a fully awake state to a stable level of hypnosis. The surgical procedure takes place during the maintenance phase of anesthesia. Once the procedure is completed, drug administration

* Corresponding author. Tel.: +46 46 222 87 92; fax: +46 46 138118.
E-mail address: kristian@control.lth.se (K. Soltesz).
[1] The authors are members of the LCCC Center and eLLIIT Excellence Center at Lund University.

1746-8094/$ – see front matter © 2013 Elsevier Ltd. All rights reserved.
http://dx.doi.org/10.1016/j.bspc.2013.04.005

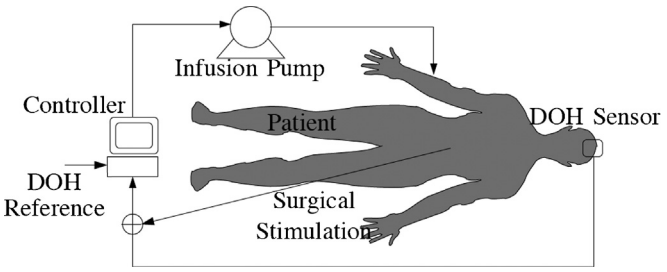

Fig. 1. Closed-loop DOH control system.

is discontinued to yield the emergence phase of anesthesia. During this phase, the patient emerges from the anesthetized state to the fully awake state.

Classically, an anesthesiologist manually controls administration of anesthetic drugs in the operating room. Doses are determined based on measured and/or predicted patient response. The predictions are based on clinical experience complemented by anticipated response to surgical stimulation and synergetic effects between drugs. Expert knowledge and experience play an important role, because the process exhibits a high degree of uncertainty.

A computer application can be used for a priori computation of an adequate hypnotic dose profile. This is exploited in the Target Controlled Infusion (TCI) paradigm [6,7]. TCI uses pharmacokinetic (PK) and pharmacodynamic (PD) models to regulate the predicted plasma or effect site (brain) drug concentration to a desired level set by the anesthesiologist. Considering that these concentrations are calculated rather than measured, TCI is regarded as an open-loop scheme. Thus, the performance of any TCI system relies heavily on the accuracy of the patient model. Furthermore, it is highly susceptible to disturbances caused by surgical stimulation and hypnotic–opioid synergy. Consequently, the TCI profile needs to be manually adjusted to counteract such disturbances.

An important step toward automated anesthesia drug delivery is to allow a computer application to make adjustments based on appropriate sensor measurements. In this scenario the anesthesiologist provides reference profiles for the measured quantity and the computer administers drugs to track the reference. This paradigm, known as closed-loop control, has been enabled with the introduction of clinical sensors for depth of hypnosis such as the Bispectral Index (BIS) [8], Entropy monitor [9] and the wavelet-based NeuroSense monitor [10]. In this paper a model of the commercially available NeuroSense monitor (NeuroWave Systems, Cleveland Heights, USA) is used. It provides the WAV_{CNS} index, presented in Section 2.3, as a measure of clinical effect. It is shown that the WAV_{CNS} correlates well with the BIS in steady state [10], and in addition, it boasts improved time-invariant dynamic response. Fig. 1 outlines the components of a closed-loop controlled anesthesia system.

The minimum requirement for any controller is that the closed-loop system is robust against measurement noise, disturbances (e.g. surgical stimulation) and model uncertainties. Improving robustness usually results in compromised controller performance and an appropriate trade-off between robustness and control performance is required. This compromise explains the existence of a multitude of control schemes and corresponding tuning procedures that have been evaluated for drug delivery in anesthesia. These schemes have included internal model control (IMC) [11], modeling error compensation (MEC) [12], model predictive control (MPC) [13], neural-fuzzy control [14], proportional integral derivative control (PID) [15] and robust control [15,16]. An intensive list of previous work on closed-loop control of anesthesia can be found in a historic review [17] and more recently in [18] as well as in [3]. It was

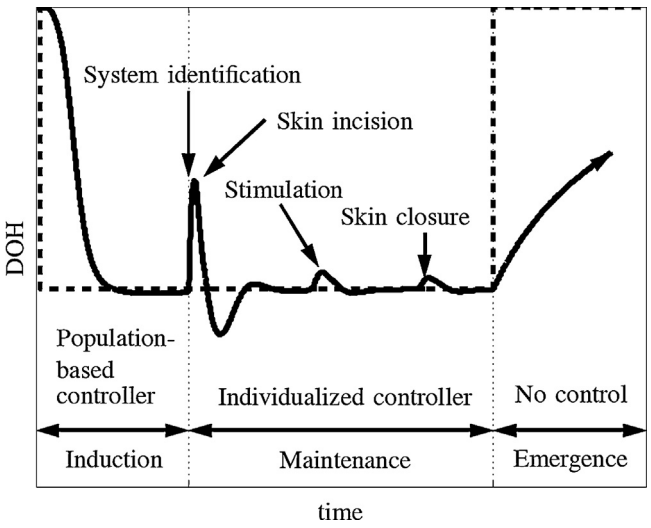

Fig. 2. Temporal layout of proposed control schema.

concluded in [19,20] that closed-loop strategies might outperform manual infusion dosing. In particular, closed-loop administration of propofol is expected to lead to a mean decrease in drug dose, while providing adequately deep anesthesia.

The output (WAV_{CNS} index provided by the NeuroSense monitor) and its corresponding input (dose) history can be used to adapt the control scheme to improve titration of drugs to the need of an individual patient. However, such adaptive approaches can fail if the behavior of the clinical front end is not fully explained by the dose, or if the output does not adequately excite the process to be controlled. In control of anesthesia, unknown surgical stimulations affect the clinical front end. With current technology, it is not possible to separate this effect from that of the drug. Hence, the clinical front end measurement is not fully explained by the dose during intubation or after incision, thereby posing a challenge for any adaptive scheme. This challenge is exacerbated by the fact that measurement noise is of comparable magnitude to output variability during the maintenance phase of anesthesia [3].

This paper proposes an individualized approach to closed-loop control of depth of hypnosis during propofol anesthesia. Its novelty lies in the individualization of the controller at the end of the induction phase of anesthesia, based on a patient model identified from dose–response relationship during induction of anesthesia. The proposed approach is superior to population-based drug administration in titrating drug to the need of each individual patient. This novel approach also has potential to outperform fully adaptive approaches in regards to controller robustness against measurement variability due to surgical stimulation. An overview of the proposed approach is given in Fig. 2.

To streamline controller synthesis, two output filters are introduced, which yield close-to-linear representation of the system dynamics when used with a compartmental patient model (the Hill dose–response model and the linear time-invariant sensor model). This synthesis is useful during the induction phase of anesthesia in which nonlinear dose–response relationship complicates the design of an appropriate controller.

This paper is organized as follows: Section 2 describes the model of hypnosis used in this paper. Section 3 elaborates on the control design procedure employed once a plant model is given, whereas the system identification procedure to obtain the plant model is discussed in Section 4. Sections 5 and 6 describe the simulation setup and performance evaluation measures. Section 7 presents and discusses the results and Section 8 outlines the limitations of the study. Section 9 provides the conclusions.

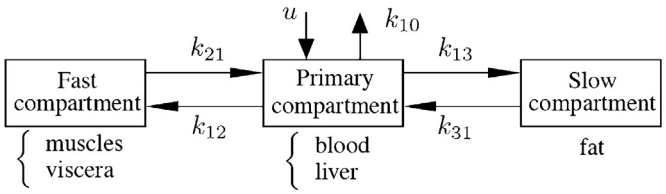

Fig. 3. Mammillary three-compartment model.

2. A dynamic model of hypnosis

The model structure used in this paper consists of a PK model [21] (explaining the distribution and elimination of the drug), a PD model [3] (explaining the clinical effect of the drug) and a model describing the monitor dynamics [10]. Surgical stimulation is modeled as an additive disturbance to the measurement signal. Each model is described in detail in the following:

2.1. Pharmacokinetic (PK) model

The PK model relates infusion rate u to plasma drug concentration Cp. A variety of PK models have previously been described, e.g. [21–24]. In this paper, the Schüttler PK model [21] was used. It is a three-compartment mammillary model in which each compartment represents a class of tissues (see Fig. 3). Propofol is delivered into the primary compartment at the infusion rate u. Drug mass in each compartment is denoted by $m = [m_1\ m_2\ m_3]^T$. Rate constants k_{ij}, $i, j \in \{1, 2, 3\}$ describe the mass fraction of propofol transported from compartment i to compartment j. Elimination takes place only from the primary compartment with the rate constant k_{10}. The compartment volumes are denoted by V_k, $k \in \{1, 2, 3\}$. These volumes are theoretical measures and do not correspond to physical volumes in the patient. The drug concentrations in each compartment are given by

$$x = [x_1\ x_2\ x_3]^T, \quad x_k = \frac{m_k}{V_k}, \quad k \in \{1, 2, 3\}. \tag{1}$$

If the concentrations in two compartments are equal, there is no net flow of drug between them. Hence,

$$\frac{V_1}{V_2}k_{12} = k_{21}, \quad \frac{V_1}{V_{32}}k_{13} = k_{31}. \tag{2}$$

Consequently, the Schüttler PK model can be expressed as the following state space representation:

$$\dot{x} = \begin{bmatrix} -(k_{10}k_{12}k_{13}) & k_{12} & k_{13} \\ k_{21} & -k_{21} & 0 \\ k_{31} & 0 & -k_{31} \end{bmatrix} x + \frac{1}{V_1}\begin{bmatrix} 1 \\ 0 \\ 0 \end{bmatrix} u. \tag{3}$$

The transfer function representation of (3) from u to x_1 is

$$G_{C_p,u}(s) = \frac{1}{V_1}\frac{(s+k_{21})(s+k_{31})}{(s+p_1)(s+p_2)(s+p_3)}, \tag{4}$$

where p_k, $k \in \{1, 2, 3\}$ relate to k_{ij} through

$$\begin{cases} p_1 + p_2 + p_3 = k_{10} + k_{12} + k_{13} + k_{21} + k_{31}, \\ p_1p_2 + p_1p_3 + p_2p_3 = k_{10}(k_{21}k_{31}) + k_{31}(k_{12}k_{21}) + k_{13}k_{21}, \\ p_1p_2p_3 = k_{10}k_{21}k_{31}, \end{cases} \tag{5}$$

which is obtained from the characteristic equation. Schüttler and Ihmsen [21] suggested that age and lean body mass were reliable demographic covariates for individualizing the volumes and rate constants in (3).

2.2. Pharmacodynamic (PD) model – Hill function

2.2.1. Effect site dynamics

The output of the PK model is C_p, the concentration of propofol in the primary compartment. However, the effect site of the drug is the brain. To account for the distribution of drug from the plasma to the effect site, the PK model is augmented by a first-order time-delayed (FOTD) system [3] that relates C_p to the effect site concentration C_e:

$$G_{Ce,Cp}(s) = \frac{k_d}{s + k_d}e^{-Ls}. \tag{6}$$

The standard PD model does not consider a time delay L, which was introduced to model the negative phase shift observed in clinical data [3].

2.2.2. Dose–response characteristics

In steady state, the relation between C_e and E is well described by the sigmoidal E_{max} function, also known as the Hill function:

$$E(C_e) = \frac{C_e^\gamma}{EC_{50}^\gamma + C_e^\gamma}. \tag{7}$$

The clinical effect E ranges from 0 to 1, where 0 and 1 correspond to fully awake and fully anesthetized states, respectively. The Hill function (7) is parameterized by EC_{50}, the C_e value corresponding to $E = 0.5$ and γ, representing the steepness of the sigmoidal curve. It can be decomposed into a series of a linear gain parameterized only in EC_{50}:

$$v(C_e) = \frac{1}{EC_{50}}C_e, \tag{8}$$

and a sigmoidal nonlinearity that is parameterized only in γ:

$$E = f(v;\gamma) = \frac{v^\gamma}{1 + v^\gamma}. \tag{9}$$

For model identification purposes, k_d in (6) and the gain in (8) are lumped together to yield the following FOTD system:

$$v(s) = \frac{1}{EC_{50}}\frac{k_d}{s + k_d}e^{-sL}C_p(s), \tag{10}$$

whereas the nonlinearity (9) is treated separately.

2.3. Clinical front end: WAV_{CNS} monitor

Depth of hypnosis (DOH) can be inferred based on characteristic frequency components of electroencephalogram (EEG), which can be measured using non-invasive electrodes mounted on the patient's forehead. The most popular option for the measurement of DOH is the BIS [25], for which commercial instrumentation equipment is available. However, BIS is not ideal for closed-loop control purposes, because the underlying proprietary algorithm exhibits highly time-varying and nonlinear behavior. The use of wavelet techniques has been proposed to overcome these challenges, yielding the WAV_{CNS} index [10]. It correlates well with BIS. Moreover, its implementation in the NeuroSense monitor [26] exhibits known time-invariant linear dynamics:

$$G_{y,E}(s) = \frac{1}{(8s+1)^2}. \tag{11}$$

The dynamics (11) are due to a known output trending filter embedded in the NeuroSense, rather than an approximation of its dynamic behavior. The lack of the time varying delay resulting from the proprietary BIS algorithm makes the NeuroSense monitor more suitable for closed-loop applications.

The WAV_{CNS} index spans 0–100, where 100 corresponds to the fully awake state, while 0 corresponds to an iso-electric EEG. In

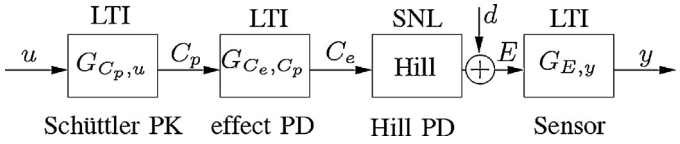

Fig. 4. PKPD patient model, relating DOH y to propofol rate u. Surgical stimulation is modeled by d.

essence, it is a scaling of y in (11) such that $y = 0 \Leftrightarrow 100\ \mathrm{WAV_{CNS}}$ and $y = 1 \Leftrightarrow 0\ \mathrm{WAV_{CNS}}$. Further details of the NeuroSense monitor can be found in [3,26].

2.4. Control design model and surgical stimulation

The patient model used for control design is obtained by combining the PK model (3), the PD model (9) and (10) and the $\mathrm{WAV_{CNS}}$ model (11); see Fig. 4. The surgical stimulation (denoted by d in Fig. 4) is modeled as an additive output disturbance. A previously published profile [15] shown in Fig. 5 is used in this simulation study. As noted in [15], this profile, though simplified, emulates three representative surgical stimulations during surgical procedures. The initial step simulates the arousal reflex due to incision. The stimulation tapers off and settles at 10 $\mathrm{WAV_{CNS}}$ units to imitate surgical interventions and finally returns to zero once the surgical stimulation is withdrawn. The profile is regarded as adequate for investigating the preliminary feasibility of the proposed individualized controller. However, the adaptation regimen for controller parameters based on the identified patient model may need to be revised before it can be used in surgical procedures involving significantly different stimulation profiles.

3. Robust PID control

This section outlines the controller structure and elaborates on the parameter tuning procedure. Directly synthesizing a controller for the combined dynamics in Fig. 4 is complicated by the model structure, which consists of two linear blocks separated by a static nonlinearity. In order to cope with this challenge, we propose two filters that cancel the Hill nonlinearity (9) and the monitor dynamics (11). Utilizing these filters linearizes the plant, thereby facilitating the control design process.

The control strategy of choice in this paper is robustly tuned PID control. PID control is a well-accepted scheme with a simple structure involving only few parameters. Its behavior is well understood and intuitive. In addition, there are tuning schemes to secure controller robustness, e.g. [27,28]. Moreover, PID control has shown to be a viable approach to applications [29] in which the controlled system exhibits monotonous step response dynamics, which is the case in this application. It is noted that achieving improved control performance with more advanced and model-based control methods may by extremely challenging for the DOH control problem at hand due to the large amount of patient-to-patient uncertainty. In this regard, PID control can be regarded as a reasonable choice.

The standard form of the PID controller is given in continuous time, and discretization is required for implementation in a digital computer. In addition, the following enhancements were made upon the standard PID control scheme to deal with challenges specific to the DOH control problem in this paper: (1) reference weighting, (2) reference pre-filtering, (3) integrator anti-windup, (4) derivative filter and (5) bumpless parameter changes. Each of these enhancements is discussed in Section 3.4.2 (Fig. 6(a) for the overall control scheme).

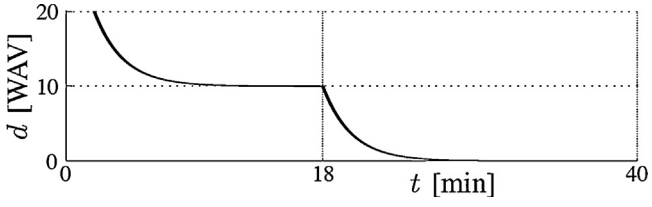

Fig. 5. Output disturbance profile from [19].

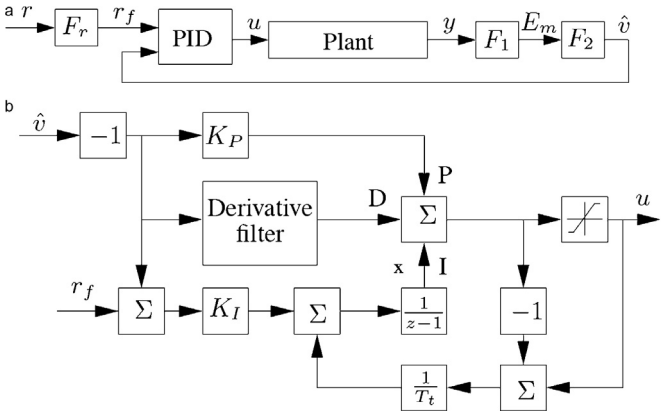

Fig. 6. Closed-loop system and PID controller.

3.1. Monitor canceling filter

The plant model shown in Fig. 4 cannot be readily decomposed into its LTI and static nonlinearity components due to the existence of the Hill function between the effect-site PD and the monitor dynamics, which acts as a significant limiting factor in both patient model identification and controller synthesis. We propose to augment the plant model with the inverse of the monitor dynamics to reduce these limitations. The monitor dynamics is the result of a trending filter, operating at 1 Hz (which is 5 times faster than the control algorithm executing with a sampling interval of 5 s). It is the zero order hold (ZOH) sampling of (11), where the unit delay from sampling has been removed:

$$G(z) = \frac{0.719z^2 + 0.662z}{z^2 - 1.765z + 0.778}. \tag{12}$$

Since (12) is stable and minimum phase, its inverse

$$F_1(z) = \frac{z^2 - 1.765z + 0.778}{0.719z^2 + 0.662z}. \tag{13}$$

is also stable and allows a causal implementation. Consequently, the output of the $\mathrm{WAV_{CNS}}$ monitor is filtered with (13) to cancel (12) (see Fig. 4).

3.2. Hill canceling filter

The model in Fig. 4 is nonlinear due to the Hill function. This is not an issue when synthesizing a maintenance phase controller, since the plant model can be linearized around the operating point where $C_e = EC_{50}$, which is known to correspond to adequate DOH. However, linear approximation is not feasible during the induction phase of anesthesia, during which no well-defined operating point exists. If a PID controller (or any controller involving integral action) is used, the integral state will build up rapidly during the beginning of the induction phase due to the large discrepancy between target and actual drug concentrations: $C_p \ll EC_{50}$, which in turn can potentially cause a large overshoot in the $\mathrm{WAV_{CNS}}$ response. Integral action may be reduced to alleviate this problem, but this would increase the duration of the induction phase. To resolve this challenge, we propose to use a linearizing filter in series with (13).

The inverse of the nonlinear part of the Hill function (9) is given by

$$v = F_2(E;\gamma) = f^{-1}(E;\gamma) = \left(\frac{E}{1-E)}\right)^{1/\gamma}. \tag{14}$$

Letting γ and $\hat{\gamma}$ be true and population-based slope parameters, respectively, yields

$$\hat{v} = f^{-1}(f(v;\gamma);\hat{\gamma}) = v^{\gamma/\hat{\gamma}}, \tag{15}$$

which is close to v when $\hat{\gamma} \approx \gamma$. The controller can be synthesized based on the assumption that $\hat{\gamma} = \gamma$, i.e. the nonlinearity is completely canceled.

3.3. Plant dynamics

Combining (4), (6), (8), (12), (13) and (15) and assuming $\hat{\gamma} = \gamma$ yields the fully linear plant model

$$P(s) = \frac{k_d}{EC_{50}V_1}\frac{(s+k_{21})(s+k_{31})}{(s+k_d)(s+p_1)(s+p_2)(s+p_3)}e^{-sL}, \tag{16}$$

which is used for controller synthesis.

3.4. Controller

The PID controller is parameterized in its proportional (K_P), integral (K_I) and derivative (K_D) gains. Two robust PID design methods based on minimizing the norm of the tracking error caused by a step load disturbance are evaluated to determine the values of these gains.

3.4.1. Robust load integrated error minimization

The objective of this method is to find PID gains $\{K_P, K_I, K_D\}$, that minimize the integral error (IE). Robustness is enforced by restricting the open-loop Nyquist curve outside a circular disk of radius M_s centered at -1. This is equivalent to restricting the ∞-norm of the sensitivity function $S(\omega)$:

$$\begin{aligned} &\{K_P, K_I, K_D\} = arg\min \int_0^\infty e_L(\tau)d\tau, \\ &\text{subject to} \max_\omega |S(\omega)| \le M_s, \end{aligned} \tag{17}$$

where e_L is the error due to a step disturbance load. See [28] for a thorough description of the method or [29] for a summary. A regimen for determining a suitable M_s is described in [15].

3.4.2. Robust load integrated absolute error minimization

An oscillatory zero mean error is not desirable, but it can yield small IE values. The following optimization constraint can be used as a remedy:

$$\begin{aligned} &\{K_P, K_I, K_D\} = arg\min \int_0^\infty e_L(\tau)d\tau, \\ &\text{subject to} \max_\omega |S(\omega)| \le M_s, \end{aligned} \tag{18}$$

The minimized quantity is referred to as the integral absolute error (IAE), where e_L is the error due to a step disturbance load. A useful algorithm to perform (18) is available in [27].

A preliminary simulation study based on closed-loop DOH control indicates that the behavior of controllers designed using (17) and (18) are essentially similar. Therefore, the IE minimization was adopted in favor of its IAE counterpart by virtue of its computational efficiency.

3.5. Implementation aspects

The standard, generic PID controller was customized as follows to accommodate specific requirements associated with the real world implementation of a DOH controller. Changes were made to accommodate integrator anti-windup and bumpless parameter changes. The reference was low-pass filtered to generate a more feasible trajectory and the derivative term was low-pass filtered to handle measurement noise.

3.5.1. Reference weighting

In this work, rejection of disturbances and suppression of oscillations in response is prioritized over tight reference tracking. Therefore, zero reference weight is chosen for the proportional and derivative terms of the PID control law, which forces the reference to enter the control signal only through the integral term of the PID control law; see the block diagram of the controller shown in Fig. 6(b).

3.5.2. Reference pre-filtering

The reference is normally changed in steps. To avoid oscillations and over-dosing during the induction phase of anesthesia, the reference was processed using the following low-pass filter:

$$F_r(s) = \frac{1}{sT_r + 1}. \tag{19}$$

This delivers a smoother and hence more feasible reference trajectory than its step-wise counterpart. The time constant T_r is chosen to make the closed-loop set point response behave like a second order system with the damping ratio of $\zeta = 0.7$ and the time constant of $\approx$5 min, as described in [30].

3.5.3. Saturation and integrator anti-windup

The control signal has a natural lower bound $u_{\min} = 0$ (since drug cannot be extracted once infused). An upper bound $u_{\max} = 3.33$ mg/s is imposed, which is based on the pump flow capacity of 1200 ml/h and the use of 10 mg/ml propofol. To prevent windup of the integrator in the PID controller, a tracking anti-windup scheme is implemented, as shown in Fig. 6(b). The tracking time constant T_t is chosen as the geometric mean of the integral ($T_I = K_P/K_I$) and derivative ($T_D = K_D/K_P$) time constants of the PID controller as recommended in [29]:

$$T_t = \sqrt{T_I T_D} = \sqrt{\frac{K_D}{K_I}}. \tag{20}$$

3.5.4. Derivative filter

To suppress high-frequency noise, the differentiator K_D is low-pass filtered through

$$\frac{1}{1 + (K_D/K_P N)s}, \tag{21}$$

which yields the filtered derivative

$$\frac{sK_P K_D N}{sK_P + K_D N}, \tag{22}$$

where $N = 5$ was chosen heuristically to yield an adequate trade-off between noise suppression and phase lead. The reference was not included in order to facilitate a smooth response to rapid and abrupt reference changes.

3.5.5. Bumpless parameter changes

Changing the gains of the PID controller at the end of the induction phase may result in discontinuity in the control signal due to the derivative in calculating the control law. To illustrate this problem, let x_I and x_D be the states associated with integrator and derivative filter in the PID controller shown in Fig. 6(b). The control signal is given by

$$u = \text{sat}_{u_{\min}}^{u_{\max}}\left(-\hat{v}K_P + x_I - \hat{v}K_P N - x_D\frac{K_P N}{K_D}\right). \tag{23}$$

It is clear that an undesired discontinuous changes in u can occur when parameters are changed from $\{K_P, K_I, K_D\}$ to $\{K'_P, K'_I, K'_D\}$. This is prevented by simultaneously updating the states as follows:

$$x'_D = \hat{v}(K'_P - K_P)\frac{K'_D}{K'_P} - x_D\frac{K_P}{K_D}\frac{K'_D}{K'_P}, \tag{24}$$

$$x'_I = x_I + \hat{v}(K'_P - K_P). \tag{25}$$

3.5.6. Discretization

The controller is discretized using the forward Euler approximation $s \approx z - 1$, which is acceptable considering that the sample period (1 s) is small compared to the dominant time scale of the system, considering that the mean PD time constant of the models presented is approximately 28 s. Using ZOH discretization or conducting tuning optimization in the discrete time domain would be possible alternatives. However, these options were not pursued in this paper since they lack the intuitive insights provided by the continuous time PID control architecture that are preserved in the proposed discretization.

4. Parameter identification

4.1. Preliminaries

Our proposed individualized control scheme uses the propofol infusion and WAV_{CNS} profiles during the induction phase of anesthesia to individualize the patient model (PD model in particular; see Fig. 4). A preliminary simulation-based analysis revealed that the system is not sufficiently excited to identify all parameters in (3), (9) and (10) simultaneously – the input is essentially a band-pass filtered step signal. In order to make system identification tractable, the FOTD system (10) can be parameterized using

$$K = \frac{1}{EC_{50}}, \quad T = \frac{1}{K_d}. \tag{26}$$

The objective of the system identification is then to identify $\{K, T, L, \gamma\}$ from (6), (9) and (26). The signals C_p and E are needed to identify the PD model (9) and (10). Because E is not directly available, its estimate E_m is used. It is obtained by applying F_1 in (13) to y (Fig. 6(a)). Likewise, an estimate C_{pm} of C_p, obtained by driving the PK model (4) with u, is used.

Since v in (9) ranges from 0 to ≈0.5 during the induction phase of anesthesia, linearizing (9) in the neighborhood of a nominal operating point is not an attractive approach to PD model identification. Moreover, it is hard to discriminate the effects of the nonlinearity parameter γ and the time delay L in the induction phase data. To illustrate this point, a closed-loop induction of anesthesia was conducted on an average patient assuming perfect knowledge of the patient model.[2] Subsequently, patient models with γ ranging from 0.2 to 4 and delay L ranging from 0 s to 70 s were driven by u_{ind}, producing a drug infusion profile during induction of anesthesia. The bounds on γ and L were chosen based on the parameter values reported in [15]. For each case, the resulting response y_{ind} was obtained and the error $||y_{ind} - y^*_{ind}||^2$, where y^*_{ind} is the true model response to u_{ind}, was computed. Fig. 7 shows the existence of a flat valley in $\gamma - L$ space that minimizes the error, which implies that the set of parameters $\{\gamma, L\}$ can drift along this valley. Therefore, this paper proposes a two-stage approach to identify the PD model based on the dose–response relationship during the induction phase of anesthesia. Such an approach allows for a conscious choice of point in the cost valley, as opposed to a simultaneous 1-stage identification procedure.

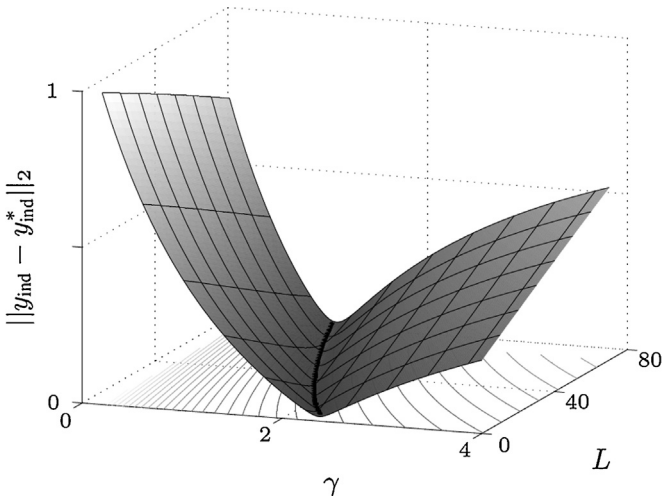

Fig. 7. Normalized L_2-norm of induction phase output error as function of T_d and γ.

4.2. Stage 1: identification of γ

Inspecting the simulated pairs of u and E reveals that the first-order dynamics is fast compared with the time scale of the induction of anesthesia. Thus, it is reasonable to approximate (10) by a delayed gain $K{\cdot}e^{-Ls}$. Based on this approximation, an initial estimate $\hat{L}$ of L can be obtained by identifying the time instant after which E_m and u remain above the thresholds $E_{m_{\sigma^-}}$ and u_σ, respectively. The last part of the induction phase of anesthesia is close to stationary. Consequently, an initial estimate $\hat{K}$ of K can be obtained by averaging the ratio of E_m and u over the last 3 min within the induction phase of anesthesia. Subsequently, the initial estimate $\hat{\gamma}$ of γ can be obtained by a bisection search to minimize (the discretized equivalent of)

$$J(\hat{\theta}) = \int_0^{t_\gamma} (f^{-1}(E_m; \hat{\gamma})(t) - KC_{pm}(t - L))^2 dt. \tag{27}$$

Fixing $\hat{\gamma}$ yields the estimate v_m of v:

$$v_m = f(E_m; \hat{\gamma}). \tag{28}$$

Finally, a bisection search is used to find the estimate $\hat{T}$ of T, which minimizes (the discretized equivalent of)

$$\int_0^{t_{ind}} \left(v_m(t) - L^{-1}\left(\frac{\hat{K}}{s\hat{T}+1} e^{-s\hat{L}} C_{pm} \right) \right)^2 dt. \tag{29}$$

4.3. Stage 2: identification of LTI parameters

A gradient-based parameter identification method [31] can be used to obtain refined estimates of the PD model parameters based on the patient's response during the induction phase of anesthesia. The parameter estimates are identified to minimize:

$$\int_0^{t_{ind}} (v_m - \hat{v})^2 dt, \tag{30}$$

where v_m is parameterized in $\hat{\theta} = \{K, T, L\}$, while $\hat{\gamma}$ is fixed to the value obtained by the initial parameter identification scheme. Computing the gradient $\nabla J(\hat{\theta})$ and an approximation of the Hessian $\nabla^2 J(\hat{\theta})$ can be done by simulating an augmented system, where the augmented states are partial derivatives of the objective

[2] The patient model was assembled from population averages for all parameters, including $\gamma^* = 2.1$ and $L^* = 14.8$ s, from which the input (u_{ind}) and output (y_{ind}) sequences were collected.

function (30) with respect to the PD model parameters to be identified. Details of the method are discussed in [31].

5. Simulation experiments

In order to validate the proposed approach to DOH control, a hypothetical surgical procedure was simulated for each patient in the test population, as described below.

5.1. Test population

The test population consisted of 44 PKPD models. Model parameters were obtained by applying a system identification procedure to the clinical data collected from real patients [15]. In the course of system identification, it was assumed that individual PK models could be accurately characterized using the covariate formulae of Schüttler [21]. This essentially lumps all the parametric uncertainty into the PD model.

5.2. Experimental layout

5.2.1. Induction phase

Prior to the simulated surgical procedure, a population-based induction phase controller was synthesized according to the procedure described in Section 3 based on the control design model (16). The PK model parameters were computed from patient age and weight using the covariate formulae by Schüttler, while population averages were used for K_d, EC_{50} and T_d.

5.2.2. PD identification and controller re-design

The PD parameters were estimated as described in Section 4. They were then used to synthesize an individualized controller at the end of the induction phase. The controller for maintenance and emergence phases was synthesized as described in Section 3.

5.3. PK uncertainty

In order to introduce realistic amount of PK uncertainty in the simulated procedure, perturbations were introduced to the parameters in the patient model. This was systematically done using normally distributed random numbers with standard deviations chosen as those of the prediction residuals reported in Schüttler and Ihmsen [21]. By drawing from these distributions, a group of 20 patient models was created for each of the 44 nominal PKPD models. The average μ and standard deviation σ of the performance measures in Section 6 below were computed within each group, using a controller based on perfect model knowledge (PM), the induction phase controller (DC) and the individualized controller (IC).

6. Performance evaluation

This section elaborates performance measures used for the evaluation of proposed approach to DOH control. Varvel et al. [32] proposed measures useful for evaluating the performance of TCI systems, which were later adopted by other closed-loop studies [33,34]. These measures are based on the median value of the error (which is robust against outliers) and thus are particularly well suited for problems in which a lot of outliers are expected. In closed-loop control, the signal fed to the controller is normally filtered a priori to remove artifacts and noise. Therefore, this paper proposes to compute the error measures directly from the control error $r - y$ rather than imposing the robustness to the measures themselves via taking median values. In fact, the measures used in this paper are well established within the control engineering community. Prior to applying these measures to the responses obtained from simulation experiments, the profiles of propofol infusion and DOH response were partitioned into induction, maintenance and emergence phases of anesthesia, which were then evaluated separately as described below.

6.1. Induction phase

6.1.1. 90% rise time (RT) [min]

The rise time is defined as the time from the start of the procedure until the DOH first reaches within 10% of the reference (i.e. 0.6).

6.1.2. Overshoot (OS) [%]

Shortening the rise time by increasing the infusion rate may lead to an over-dose, resulting in an overshoot in DOH response. The overshoot is the percent difference between the lowest DOH and the DOH reference.

6.2. Maintenance phase

6.2.1. Integral absolute error (IAE) [WAV]

The IAE is defined as:

$$\mathrm{IAE} = \frac{1}{T}\int_0^T |e(t)|dt, \tag{31}$$

which can be interpreted as the average absolute error.

6.2.2. Integral error (IE) [WAV]

The IE is similar to the IAE, but lacking the modulus:

$$\mathrm{IE} = \frac{1}{T}\int_0^T e(t)dt, \tag{32}$$

which can be regarded as a measure of average bias.

6.2.3. Standard error (SE) [WAV]

The SE is the standard deviation of the error profile. It captures variability not seen in the IAE or IE. It may be desirable to have a somewhat larger IAE but smaller SE, e.g. imperfect tracking with small oscillations (which is consistent with the control objective states in Section 3).

7. Results and discussion

The novelty of the proposed approach to DOH control lies in adapting the controller gains to each individual patient at the end of the induction phase of anesthesia, based on a model identified from the patient's dose–response relationship during induction of anesthesia. It provides individualization of the controller gains to better titrate propofol to the need of an individual patient, while avoiding identifiability challenges caused by immeasurable surgical stimulation that could compromise a continuous adaptation approach.

Table 1 summarizes the performance measures computed for the surgical procedures simulated with the disturbance profile shown in Fig. 5. The corresponding DOH and propofol infusion profiles for the individualized control are presented in Fig. 8, where each line corresponds to the response of individual patient, with the PK parameter disturbances drawn as described in Section 5.3. Overall, the results were consistent with what was expected – PM showed the best performance, followed by IC and then DC. What is more promising is that the difference in performance between PM and IC was marginal. In terms of mean values, RT and OS were smaller for PM than DC (with significance $p < 0.05$, using the Student's unpaired t-test), which suggests that incorporating accurate

Table 1
Rise tome (RT), overshoot (OS), Integral absolute error (IAE), integral error (IE) and standard error (SE) means (μ) and standard deviations (σ) for the perfect model knowledge (PM), demographics-based (DC) and individualized (IC) control.

		RT	US	IAE	IE	SE
PM	μ	7.02	1.42	1.08	0.15	2.63
	σ	0.36	0.88	0.42	0.14	0.56
DC	μ	7.11	1.62	1.57	0.16	3.44
	σ	0.36	0.96	0.51	0.15	0.61
IC	μ	7.11	1.62	1.17	0.18	2.76
	σ	0.36	0.96	0.45	0.15	0.59

knowledge of the PKPD model into the control scheme can indeed improve the quality of closed-loop drug delivery. For IAE, IE and SE, it was found that PM < IC < DC ($p < 0.05$), with the following exception: IE was larger for IC than DC (with significance; $p < 0.05$). Noting that (1) disturbance rejection and elimination of oscillations were given higher priority than fast reference tracking, and (2) a large reduction in IAE was achieved at the cost of a slight deterioration in IE, this result is deemed acceptable. The mean IAE decrease from DC to IC of 25% provides a representative measure of performance improvement that can be achieved by individualized control.

It is noted that the proposed individualization approach with the controller gain adaptation may need to be modified and optimized for the given surgical procedure so that the challenges associated with particular surgical procedure can be readily accommodated. For instance, larger DOH overshoots can be tolerated in surgeries where mechanical ventilation is employed, as opposed to ones during which the patient breathes spontaneously. However, this does not hold for fragile or elderly patients. The problem of procedure- or patient category specific gain tuning design was not explored in this paper because its main purpose was to demonstrate the superiority of the individualized control as it is compared with population-based control.

8. Limitations and future work

Despite promising preliminary findings, this study has a number of limitations as listed below.

Firstly, it was assumed that a patient's PK can be perfectly described by the Schüttler's PK model, which in reality is not achieved. The inaccuracy of the PK model can lead to limited fidelity of the associated PD model [35]. For example, a PK model that has faster dynamics than the response of a real patient may be compensated by identifying a PD model that has slow dynamics. However, a PK model with slower dynamics than the response of a real patient may not be compensated with PD model identification due to the causality requirement. In this regard, the physiologic implications of the PD model parameters obtained from the proposed system identification procedure may have reduced accuracy since they are partially responsible for minimizing the discrepancy between the PK of a simulated patient and the corresponding Schüttler's PK model. In any case, the results from this paper suggest that the PD model thus identified is adequate for the design of an individualized controller.

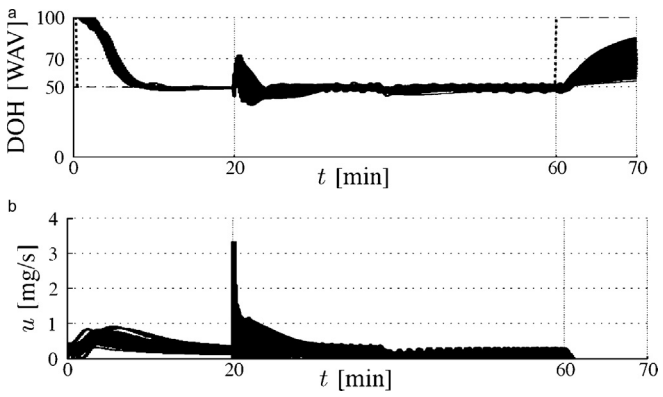

Fig. 8. Measured DOH and infusion profiles of the test population.

Secondly, the impact of measurement noise and/or artifact due to surgical stimulation and patient movement was not fully investigated. In the real clinical environment, the controller must operate in the presence of poor signal quality. It is, therefore, necessary to thoroughly understand how these confounders can affect the proposed approach. In particular, the effect of measurement noise and possible signal loss during the induction phase of anesthesia needs to be rigorously quantified. Although surgery takes place during the maintenance phase, stimulation artifacts during induction of anesthesia are not uncommon. Such artifacts could strongly bias identification and thus need to be detected.

Thirdly, the findings presented in this paper must be further validated by experimental investigations. This paper is intended to be a preliminary feasibility study. As such, focus was given to investigating the potential of the proposed approach to enhance the performance of DOH control based on realistic simulation scenarios. Our results clearly suggest promise, but the extent of performance improvement and its characteristics may vary with factors such as (1) mismatch between population-based patient models (e.g. Schüttler's PK model) and the response characteristics of real patients and (2) the nature of surgical stimulation during the procedure. Therefore, further validation of the proposed approach must be based on real patient responses under a range of surgical procedures. Particularly, the feasibility of patient model parameter identification from clinical induction phase data needs to be validated.

9. Conclusion

A robust individualized approach was proposed for closed-loop depth of hypnosis control with propofol. This novel approach can adapt the controller to individual patients to achieve desired control performance even in the presence of large inter-individual variability in hypnotic response to propofol. A comprehensive simulation-based study was conducted to assess the performance of the proposed approach with respect to the existing population-based control. The individualized approach outperformed its population-based counterpart with improvement in a variety of performance measures with statistical significance.

References

[1] S. Bibian, C.R. Ries, M. Muzmezan, G.A. Dumont, Introduction to automated drug delivery in clinical anesthesia, European Journal of Control 11 (6) (2005) 535–537.
[2] J.-O. Hahn, S. Khosravi, G.A. Dumont, J.M. Ansermino, Two-stage vs mixed-effect approach to pharmacodynamic modeling of propofol in children using state entropy, Pediatric Anesthesia 21 (2011) 691–698.
[3] S. Bibian, Automation in clinical anesthesia, Department of Electrical and Computer Engineering, University of British Columbia, Vancouver, Canada, 2006 (Ph.D. Thesis).
[4] S.E. Kern, X. Guoming, J.L. White, T.D. Egan, Opioid–hypnotic synergy: a response surface analysis of propofol-remifentanil pharmacodynamic interaction in volunteers, Anesthesiology 100 (6) (2004) 1374–1381.
[5] M. Tramer, A. Moore, H. McQua, Propofol anesthesia and post-operative nausea and vomiting: quantitative systematic review of randomized controlled studies, British Journal of Anesthesia 78 (1997) 247–255.
[6] J.B. Glen, The development of diprifusor: a TCI system of propofol, Anesthesia 53 (1998) 13–21.
[7] G.E.V. Pouke, L.J.B. Bravo, S.L. Shafter, Target controlled infusions: targeting the effect site while limiting peak plasma concentration, IEEE Transactions on Biomedical Engineering 51 (2004) 1869–1875.
[8] J. Liu, H. Singh, P. White, Electroencephalographic bispectral index correlates with intraoperative recall and depth of propofol-induced sedation, Anesthesia and Analgesia 84 (1997) 185–189.

[9] H. Viertö-Oja, et al., Description of the entropy algorithm as applied in the Datex-Ohmeda S/5 entropy module, Acta Anaesthesiologica Scandinavica 48 (2) (2004) 154–161.
[10] T. Zikov, S. Bibian, G. Dumont, M. Huzmezan, C. Ries, Quantifying cortical activity during general anesthesia using wavelet analysis, IEEE Transactions on Biomedical Engineering 53 (4) (2006) 617–632.
[11] A. Gentilini, et al., Modeling and closed-loop control of hypnosis by means of bispectral (BIS) with isoflurane, IEEE Transactions on Biomedical Engineering 48 (2001) 874–889.
[12] H. Puebla, J. Alvarez-Ramirez, A cascade control approach for hypnosis, Annals of Biomedical Engineering 33 (2009) 1449–1463.
[13] Y. Sawaguchi, E. Furutani, G. Shirakami, M. Araki, K. Fukuda, A model-predictive hypnosis control system under total intravenous anesthesia, IEEE Transactions on Biomedical Engineering 55 (2008) 874–887.
[14] M. Mahfouf, C.S. Nunes, D.A. Linkens, J.E. Peacock, Modeling and multivariable control in anesthesia using neural-fuzzy paradigms part II. Closed-loop control of simultanous administration of propofol and remifentanil, Artificial Intelligence in Medicine 35 (2005) 207–213.
[15] G.A. Dumont, A. Martinez, M. Ansermino, Robust control of depth of anesthesia, International Journal of Adaptive Control and Signal Processing 23 (2009) 435–454.
[16] J.-O. Hahn, G.A. Dumont, J.M. Ansermino, Robust closed-loop control of hypnosis with propofol using WAV_{CNS} index as the controlled variable, Biomedical Signal Processing and Control 7 (September (5)) (2012) 517–524.
[17] R. Chilcot, A review of the control of depth of anaesthesia, Transactions of the Institute of Measurement and Control 2 (January (1)) (1980) 38–45.
[18] G.A. Dumont, Closed-loop control of anesthesia – a review, in: 8th IFAC Symposium on Biological and Medical Systems, Budapest, Hungary, 2012.
[19] N. Liu, et al., Titration of propofol for anesthetic induction and maintenance guided by the bispectral index: closed-loop versus manual control, Anesthesiology 104 (2006) 686–695.
[20] N. Liu, et al., Closed-loop coadministration of propofol and remifentanil guided by bispectral index: a randomized multicenter study, Anesthesia and Analgesia 2011 (2011) 546–557.
[21] J. Schüttler, H. Ihmsen, Population pharmacokinetics of propofol: a multicenter study, Anesthesiology 92 (2000) 727–738.
[22] B. Marsh, M. White, N. Morton, G.N. Kenny, Pharmacokinetic model driven infusion of propofol in children, British Journal of Anaesthesia 67 (1991) 41–48.
[23] T. Schnider, et al., The influence of method of administration and covariates on the pharmacokinetics of propofol in adult volunteers, Anesthesiology 88 (1998) 1170–1182.
[24] L.B. Sheiner, D.R. Stanski, S. Vozeh, R.D. Miller, J. Ham, Simultaneous modeling of pharmacokinetics and pharmacodynamics: application to d-tubocurarine, Clinical Pharmacology and Therapeutics 25 (1979) 358–371.
[25] J.W. Johansen, P.S. Sebel, Development and clinical application of electroencephalographic bispectrum monitoring, Anesthesiology 93 (2000) 1336–1344.
[26] S. Bibian, G.A. Dumont, T. Zikov, Dynamic behavior of BIS, M-entropy and neuroSENSE brain function monitors, Journal of Clinical Monitoring and Computing 25 (November (1)) (2010) 81–87.
[27] O. Garpinger, T. Hägglund, A software tool for robust PID design, in: Proc. 17th IFAC World Congress, Seoul, Korea, 2008.
[28] H. Panagopoulos, K.J. Åström, T. Hägglund, Design of PID controllers based on constrained optimisation, IEEE Proceedings of the Control Theory & Applications 149 (2002) 32–40.
[29] K.J. Åström, T. Hägglund, Advanced PID Control, ISA, 2006.
[30] A. Martinez, Robust control: PID vs fractional control design, a case study, University of British Columbia, Vancouver, Canada, 2005 (Master's Thesis).
[31] K. Soltesz, T. Hägglund, K.J. Åström, Transfer function parameter identification by modified relay feedback, in: Proc. American Control Conference, Baltimore, USA, 2010.
[32] J.R. Varvel, D.L. Donoho, S.L. Shafer, Measuring the predictive performance of computer-controlled infusion pumps, Journal of Pharmacokinetics and Biopharmaceutics 20 (1992).
[33] M. Kansanaho, K.T. Olkkola, Performance assessment of an adaptive model-based feedback controller: comparison between atracurium, mivacurium, rocuronium and vecuronium, International Journal of Clinical Monitoring and Computing 13 (1997) 217–224.
[34] M.M.R.F. Struys, et al., Comparison of closed-loop controlled administration of propofol using bispectral index as the controlled variable versus standard practice controlled administration, Anesthesiology 95 (2001).
[35] S. Khosravi, J.-O. Hahn, G.A. Dumont, J.M. Ansermino, A monitor-decoupled pharmacodynamic model of propofol in children using state entropy as clinical endpoint, IEEE Transactions on Biomedical Engineering 59 (March (3)) (2012) 736–743.